

MolGraph: a Python package for the implementation of small molecular graphs and graph neural networks with TensorFlow and Keras

Alexander Kenschaft^{1,2,*}, Gert Desmet² and Deirdre Cabooter¹

(1) University of Leuven (KU Leuven), Department for Pharmaceutical and Pharmacological Sciences, Pharmaceutical Analysis, Herestraat 49, 3000 Leuven, Belgium

(2) Vrije Universiteit Brussel (VUB), Department of Chemical Engineering, Pleinlaan 2, 1050 Brussel, Belgium

(*) corresponding author:
e-mail: alexander.kenschaft@gmail.com

Abstract

Molecular machine learning (ML) has proven important for tackling various molecular problems, including the prediction of protein-drug interactions and blood brain-barrier permeability. Since relatively recently, so-called graph neural networks (GNNs) have been implemented for molecular ML, showing comparable or superior performance to descriptor-based approaches. Although various tools and packages exist to apply GNNs for molecular ML, a new GNN package, named MolGraph (<https://github.com/akenschaft/molgraph>), was developed in this work with the motivation to create GNNs highly compatible with the TensorFlow and Keras application programming interface (API). As MolGraph focuses specifically and exclusively on molecular ML, a chemistry module was implemented to accommodate the generation of molecular graphs — which could then be inputted to the GNNs for molecular ML. To validate the GNNs, they were benchmarked against the datasets of MoleculeNet, as well as three chromatographic retention time datasets. The results on these benchmarks show that the GNNs performed as expected. Additionally, the GNNs proved useful for molecular identification and improved interpretability of chromatographic retention data.

Keywords: Deep learning, machine learning, cheminformatics, bioinformatics, chemistry, chromatography, software.

Introduction

Molecular machine learning (ML) has been important in solving various molecular problems; these include prediction of aqueous solubility¹, binding of drugs to specific target proteins² and blood brain-barrier permeability³. Specifically, molecular ML tackles these problems by linking structural information (these could be descriptors⁴ or molecular fingerprints⁵) to some label (e.g., aqueous solubility measurements, binding or no binding to a protein, or permeability). As molecules are naturally represented as graphs $G = (V, E)$, where V is a set of vertices (or nodes) corresponding to the atoms, and E a set of edges corresponding to the bonds, it is strongly desired to encode molecules as graphs. By then subjecting these molecular graphs to graph neural networks^{6,7} (GNNs), highly expressive and meaningful numerical representations of molecules for downstream classification or regression tasks can be obtained. As the application of GNNs for molecular ML has already proven useful for both predictive modeling^{6–10} and interpretability^{9,11}, it was desired to develop a Python package, MolGraph (<https://github.com/akensert/molgraph>), for building GNNs specifically for those purposes (Figure 1). Importantly, as MolGraph is built to be highly compatible with the TensorFlow¹² (TF) and Keras¹³ application programming interface (API), a GNN model can be built and utilized with ease.

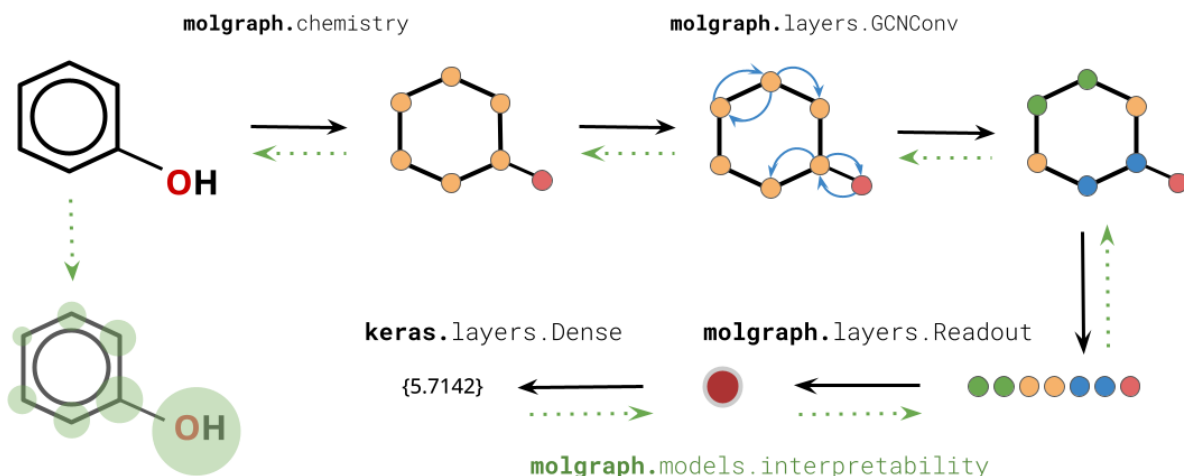


Figure 1. Schematic visualization of the different modules of MolGraph, and how they are utilized for molecular ML.

Related works and motivation

Many ML libraries exist in Python, these include Scikit-learn (for implementing classical ML models such as random forest, gradient boosting, multi-layer perceptrons, support vector machines, etc.), TF, Keras and Pytorch¹⁴ (for implementing deep neural networks). Built on top of these libraries, people have developed Python packages that specialize in certain applications. For instance, for GNN applications, these include Spektral¹⁵ (based on Keras/TF), Deep Graph Library¹⁶ (based on PyTorch, TF and Apache MXNet), DeepChem¹⁷ (based on Keras/TF and PyTorch), PyTorch Geometric¹⁸, and Graph Nets¹⁹ (based on TF and Sonnet). In contrast to the aforementioned Python packages, MolGraph focuses exclusively on GNN applications for small molecular graphs, and therefore specializes in the generation of these graphs. Additionally, MolGraph is developed with the aim to be integrated seamlessly with the TF and Keras API. This includes compatibility with the Keras *Sequential* and *Functional* model API, and TF's *SavedModel* and *Dataset* API.

Both DeepChem (a prominent Python package for molecular ML) and Spektral (a prominent Python package for GNN applications) have a broader focus than MolGraph and thus a larger set of tools and utilities. While DeepChem implements its own dataset and model API, MolGraph relies directly on the dataset and model API of TF and Keras. Although the latter requires knowledge of TF and Keras, it allows for greater flexibility, where MolGraph’s modules (mainly its *layers* module) can be used with TF’s and Keras’ existing modules to tailor GNN implementations to the specific need of the user. Spektral, like MolGraph, relies (at least in part) on the model API of TF and Keras. However, while Spektral implements four different *Data modes*, depending on the problem at hand, MolGraph only implements one: the *graph tensor*. The graph tensor is indexable, conveniently updatable, batchable, and easily convertible between batches of (sub)graphs and a single disjoint graph — both of which can be passed to a Keras model, comprising GNNs. Ultimately, MolGraph is implemented to reduce cognitive load.

API

Graph tensor

To make MolGraph compatible with TF, it was important to define an appropriate Tensor class (namely, `GraphTensor`; from hereon referred to as *graph tensor*) that can hold graph data (specifically molecular graphs). The graph tensor has two “configurations”: a “ragged” and a “non-ragged” configuration (see explanation later). The former makes the graph tensor batchable, while the latter makes the graph tensor efficient for the GNN. Specifically, the graph tensor contains nested tensors, either ragged or non-ragged, which together encode a [molecular] graph. These nested tensors include:

- **[Required]** a sparse adjacency matrix, represented as two vectors (tensors) indicating the indices of the destination nodes and source nodes. Row j corresponds to row j of *edge features* (below); and entry (index) i corresponds to row i of *node features* (below).
- **[Required]** node features (or *node states*).
- **[Optional]** edge features (or *edge states*).
- **[Optional]** graph indicator (wherein each entry indicates which graph the node belongs to, relevant for the non-ragged configuration). Row i corresponds to row i of node features.
- **[Optional]** a positional encoding. Row i corresponds to row i of node features.

The graph tensor implements methods (specifically, *merge* and *separate*) to go between the two configurations; and an *update* (and *remove*) method that allows to update (and remove) the nested tensors within the graph tensor. For the ragged configuration, the graph tensor separates each subgraph (molecule), causing the second dimension of the nested tensors to be ragged (as the molecules have different numbers of nodes/edges); for the non-ragged configuration, all subgraphs are merged into a single disjoint graph, separable by the graph indicator.

Molecular graph

The initial state of the graph tensor is computed via the *chemistry* module of MolGraph, wherein a *molecular encoder* transforms string representations of molecules (e.g., SMILES or InChI) to a molecular graph encoded as a graph tensor. Internally, the node (atom) and edge (bond) features are computed from *atomic encoders* based on a set of *features* (Table 1). As atoms of a molecule may be assigned 3D coordinates, MolGraph also supplies a molecular encoder to compute, in addition to the required sparse adjacency matrix and node features, the distance geometry of a molecule. Specialized GNNs, such as DTNN²⁰, can then exploit such information to generate a potentially improved representation of the molecule (for downstream regression or classification tasks).

Table 1. List of available atom and bond features of MolGraph.

Atom features	Bond features		
Description	Recommended encoding	Description	Recommended encoding
Chiral center	Binary	Bond type	One-hot
Chirality ('R', 'S' or None)	One-hot	Conjugated	Binary
Crippen Log P contribution	Float	Rotatable	Binary
Crippen Molar refractivity contribution	Float	Stereo	One-hot
Degree	One-hot	(Part of ring)	Binary
Formal charge	One-hot	(Part of ring of size n)	One-hot
Gasteiger charge	Float		
Hybridization	One-hot		
Aromatic	Binary		
Hydrogen donor	Binary		
Hydrogen acceptor	Binary		
Hetero	Binary		
Part of ring	Binary		
Part of ring of size n	One-hot		
Labute accessible surface area contribution	Float		
Number of hydrogens	One-hot		
Number of radical electrons	One-hot		
Number of valence electrons	One-hot		
Symbol (atom type)	One-hot		
Topological polar surface area contribution	Float		

GNN layers

Similar to how a feed-forward neural network (FFNN) is usually a stack of fully-connected layers, a GNN is usually a stack of *GNN layers*. Although the GNN layers of MolGraph take many shapes and forms, they are interchangeable, making it easy to replace one GNN layer with another. These GNN layers simply take as input a graph tensor (containing [at least] a sparse adjacency matrix and a set of node features), and outputs a new graph tensor with an updated set of node features.

In essence, the GNN layers operate in two steps: (1) transformation of the node features and (2) aggregation of the node features (based on the sparse adjacency matrix). In the simplest case, the transformation is a single linear transformation via a learnable weight matrix on the node features, directly followed by an aggregation, by averaging, for each destination node, all source nodes' features. For some of the GNN layers however, these two steps are more complicated, wherein the updated node features might depend on the relevant edge features and/or an attention mechanism.

The GNN layers of MolGraph can be separated into three different categories: convolutional (e.g., GCN^{21,22} and GIN^{22,23}), attentional (e.g., GAT^{22,24} and GMM^{22,25}) and message passing (e.g., MPNN⁸) (see Figure 2). Convolutional layers perform an arbitrary transformation ψ on the node states, and subsequently aggregate neighboring node states $j \in N_i$ to node i via normalization coefficients c_{ij} , as follows:

$$h_i^{(l+1)} = \sigma \left(\sum_{j \in N(i)} c_{ij} \psi(h_j^{(l)}) \right), \quad (1)$$

Where σ is a non-linear activation function, e.g., ReLU.

The attentional layer adds an attention mechanism, as a replacement for c_{ij} :

$$h_i^{(l+1)} = \sigma \left(\sum_{j \in N(i)} \alpha_{ij}^{(l)} \psi(h_j^{(l)}) \right), \quad (2)$$

where α denotes the attention coefficients, computed based on $h_i^{(l)}$ and $h_j^{(l)}$:

$$\alpha_{ij}^{(l)} = a(h_i^{(l)}, h_j^{(l)}), \quad (3)$$

and a is a function which computes the attention coefficients $\alpha_{ij}^{(l)}$.

The message-passing layer uses a so-called message-function which computes the “message” to be propagated to the target nodes. Specifically, in comparison with the attentional (and convolutional) approach, the message-passing approach does not pass $h_j^{(l)}$ directly, but indirectly, through the message-function; which computes the message based on $h_i^{(l)}$ and $h_j^{(l)}$:

$$h_i^{(l+1)} = \sigma \left(\sum_{j \in N(i)} \psi(h_i^{(l)}, h_j^{(l)}) \right) \quad (4)$$

As can be seen, the transformation function ψ depends on both $h_i^{(l)}$ and $h_j^{(l)}$, and not only $h_j^{(l)}$, which makes this approach most expressive.

In addition to the above, a given GNN layer may implement edge states $e_{ij}^{(l)}$ in addition to the node states; where i and j indicate that it is the edge state of the edge between node i and j . For example, the graph attention network (GAT) of MolGraph optionally incorporates edge states, wherein the attention coefficients $\alpha_{ij}^{(l)}$ are computed based on both the node states and the associated edge state:

$$\alpha_{ij}^{(l)} = a(h_i^{(l)}, h_j^{(l)}, e_{ij}^{(l)}), \quad (5)$$

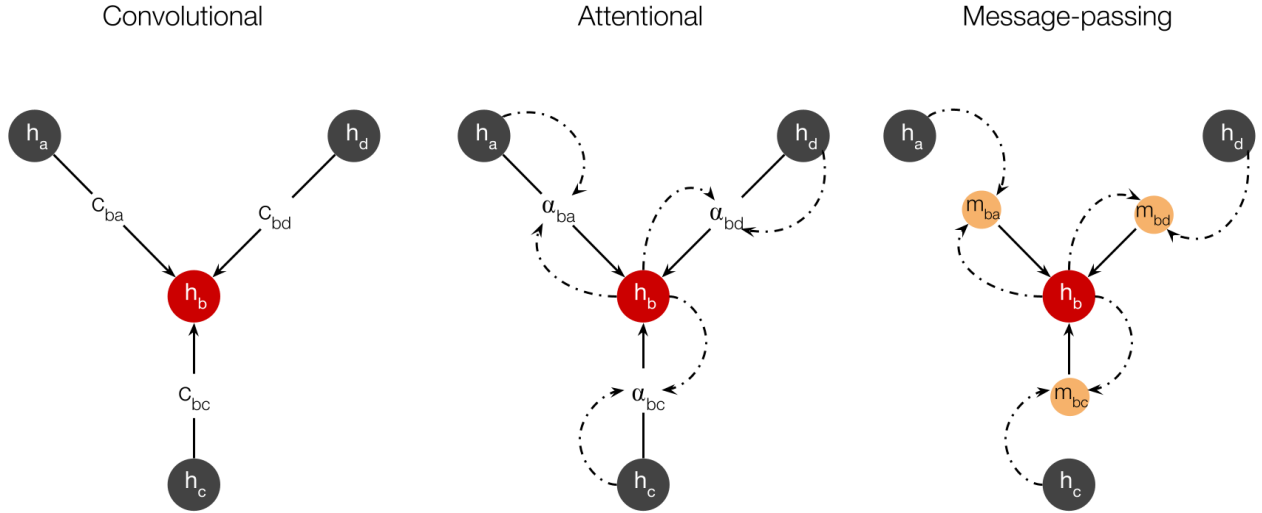


Figure 2. Schematic illustration of the three main types of graph neural networks.

Readout

After L steps of transformation and aggregation, $h_i^{(L)}$ is obtained for all nodes i in the [molecular] graph, $h_i^{(L)}$ can be used to perform e.g., node predictions, edges predictions or graph predictions. For graph (molecule) predictions, node representations $h^{(L)} \in R^{m \times k}$ (where m is the number of nodes and k the number of features) need to be reduced to a one-dimensional vector representation $z \in R^k$ of the graph (molecule). MolGraph implements several different layers that perform this reduction (known as *readout* layers). The most basic readout layer simply sums over the nodes (dimension m) as follows:

$$z_k = \sum_{i \in m} h_{ik}^{(L)}, \quad (6)$$

Subsequently, z can be passed to a FFNN (denoted f_θ) to get a prediction (denoted \hat{y}):

$$\hat{y} = f_\theta(z) \quad (7)$$

GNN models

Classification and regression

As the GNN layers can be implemented with either Keras’ functional API, sequential API, or via subclassed models, GNN models for classification and regression can both easily and flexibly be created. The *fit*, *evaluate* and *predict* methods of these models then accept either a graph tensor or a TF *Dataset* constructed from a graph tensor. Importantly, to allow for batching, the graph tensor needs to be in its ragged configuration.

Saliency and gradient activation maps

There is an increasing interest in better understanding and interpreting deep learning models (including GNNs). Among many techniques that can be used for this purpose, two prominent and well researched techniques are saliency and gradient activation mapping¹¹. To allow better understanding and interpretability of the GNNs, both saliency and gradient activation maps are implemented in MolGraph. These two techniques can be used to better understand what molecular substructures are important for the prediction; in other words, what parts of the molecules the GNN is “looking”.

Tensorflow records

For the purpose of allowing larger datasets (exceeding 50 or 100 thousand molecules), which may not fit into memory (RAM), a TF *Records* module is implemented in MolGraph. In brief, TF records allow the user to save data to disk, which can then efficiently be read (from disk) for modeling. Hence, the user may write data, namely molecular graphs (graph tensors) and associated labels, as TF records, which can then be read in a computationally and memory efficient way later on. Depending on the size of the molecular graph, as well as the computational resources, it may take anything from approximately 30 to 300 seconds to write 100 thousand small molecular graphs to TF record files; reading the TF records is significantly faster.

Experiments and results

Predictive performance

To verify and evaluate the different GNNs, they were implemented with the Keras sequential model API, and subsequently fitted to, and evaluated on, a selection of benchmarks (datasets). The benchmarks included 15 datasets from MoleculeNet²⁶, one dataset from Domingo-Almenara et al.²⁷ (in this study, referred to as “SMRT”; an abbreviation for *small molecular retention times*), and two datasets from Bonini et al.²⁸ (in this study, referred to as “RPLC” and “HILIC”; reflecting which chromatographic separation mode was used, namely, *reversed-phase liquid chromatography* and *hydrophilic interaction liquid chromatography*). To get a better understanding of how well these GNNs performed, evaluation metrics were compared between the models of this study and the original publications of the benchmarks (referenced above). Importantly, the exact train, validation and test splits *could not* be extracted from the original publications (except for RPLC and HILIC), and thus exact conclusions cannot be drawn about which models performed better or worse. Instead, the comparisons give an indication of whether the models of this study (MolGraph) performed as expected. Furthermore, no hyper-parameter search was performed for any of the models of

MolGraph, due to limited computational resources. Hence, the default hyperparameters were used for the GNNs. For optimization, Adam²⁹ was used, with a starting learning rate of 0.0001 and ending learning rate of 0.000001, which decayed, on every plateau (defined as no improvement for 10 epochs), by a factor of 0.1. The training stopped when no improvement was made for 20 epochs, wherein the weights of the best epoch were restored for evaluation (on the test sets). The loss functions used were, for classification, binary cross entropy (BCE); and for regression, depending on the evaluation metric, mean absolute error (MAE), root mean squared error (RMSE) or Huber.

Table 2. Predictive performance on the three quantum-chemistry datasets and three physical-chemistry datasets. Bold vs. italic named models visually separate the models (and results) of this study (MolGraph) and models (and results) of other studies (see footnote of table). “(E)” indicates that edge features were used. MAE stands for mean absolute error. RMSE stands for root mean squared error. Convolutional type models: GCN, RGCN(E), GIN, and GraphSage; attentional type models: GAT, GAT(E), GatedGCN, GatedGCN(E), GMM, GT, and GT(E); and message-passing type models: MPNN(E).

	quantum-chemistry			physical-chemistry		
	qm7 (MAE)	qm8 (MAE)	qm9 (MAE)	esol (RMSE)	lipophilicity (RMSE)	freesolv (RMSE)
GCN	18.9011	0.0086	2.4795	0.5682	0.5412	0.8453
RGCN(E)	13.6039	0.0086	2.0556	0.5992	0.5639	1.3143
GIN	19.2505	0.0084	2.0315	0.5865	0.5381	0.9066
GraphSage	20.4176	0.0092	2.4739	0.5919	0.5449	1.6146
GAT	22.0590	0.0088	2.6678	0.6471	0.5380	1.0123
GAT(E)	17.9556	0.0087	2.1902	0.5961	0.5402	5.8820
GatedGCN	12.2210	0.0088	2.3740	0.5914	0.5253	1.1264
GatedGCN(E)	10.2520	0.0088	1.9858	0.5755	0.5422	1.4468
GMM	18.5327	0.0091	2.4415	0.5453	0.5417	0.8613
GT	11.1366	0.0101	2.2205	0.6713	0.6195	1.0952
GT(E)	7.5603	0.0095	1.7375	0.6992	0.5703	1.1807
MPNN(E)	16.0046	0.0086	2.4794	0.5690	0.5183	0.9527
DTNN	10.8403	0.0114	1.3970	-	-	-
<i>GC</i> [*]	77.90	<i>0.0148</i>	4.7	0.97	0.655	1.40
<i>MPNN</i> [*]	-	<i>0.0143</i>	3.2	0.58	0.719	1.15
<i>DTNN</i> [*]	8.8	<i>0.0169</i>	2.4	-	-	-

* The exact dataset splits producing these results may differ from the dataset splits of this study. However, the same splitting strategies (including the same portions) were used. Furthermore, although these models were fitted to, and predicted on, each dataset three times, only the mean values are reported. Values are directly extracted from the MoleculeNet paper²⁶.

Table 3. Predictive performance on the four biophysics datasets and five physiology datasets. Bold vs. italic named models visually separate the models (and results) of this study (MolGraph) and models (and results) of other studies (see footnote of table). “(E)” indicates that edge features were used. ROC-AUC denotes area under the receiver operating characteristic curve. PRC-AUC denotes area under the precision-recall curve. Convolutional type models: GCN, RGCN(E), GIN, and GraphSage; attentional type models: GAT, GAT(E), GatedGCN, GatedGCN(E), GMM, GT, and GT(E); and message-passing type models: MPNN(E).

	biophysics				physiology				
	mu v (PRC-AUC)	hi v (ROC-AUC)	pc ba (PRC-AUC)	ba ce (ROC-AUC)	cl intox (ROC-AUC)	si der (ROC-AUC)	to ecast (ROC-AUC)	to x21 (ROC-AUC)	bb bp (ROC-AUC)
GCN	0.0373	0.7964	0.1387	0.8111	0.7800	0.6230	0.7472	0.8233	0.6872
RGCN(E)	0.0377	0.7945	0.1478	0.8213	0.7268	0.6583	0.7501	0.8209	0.6948
GIN	0.0033	0.7677	0.1524	0.8231	0.8188	0.6202	0.7447	0.8420	0.6763
GraphSage	0.0331	0.7763	0.1345	0.8129	0.8320	0.6376	0.7357	0.8264	0.6969
GAT	0.0308	0.8009	0.1450	0.8294	0.7515	0.6091	0.7413	0.8336	0.7196
GAT(E)	0.0279	0.7756	0.1500	0.7806	0.7483	0.6204	0.7342	0.8151	0.6938
GatedGCN	0.0693	0.7669	0.1475	0.8063	0.7754	0.5995	0.7397	0.8348	0.6807
GatedGCN(E)	0.0160	0.7689	0.1482	0.7974	0.8746	0.6302	0.7384	0.8287	0.6967
GMM	0.0380	0.7643	0.1466	0.7732	0.8128	0.6280	0.7473	0.8283	0.6903
GT	0.0034	0.7493	0.1356	0.7325	0.8322	0.5704	0.7309	0.8057	0.6857
GT(E)	0.0145	0.7543	0.1404	0.7958	0.8430	0.5922	0.7264	0.7982	0.6726
MPNN(E)	0.0542	0.7764	0.1455	0.8166	0.8109	0.6125	0.7405	0.8311	0.7107
<i>GC</i> [*]	<i>0.046</i>	<i>0.763</i>	<i>0.136</i>	<i>0.783</i>	<i>0.807</i>	<i>0.638</i>	<i>0.716</i>	<i>0.829</i>	<i>0.690</i>
<i>Weave</i> [*]	0.109	0.703	-	0.806	0.832	0.581	0.742	0.820	0.671

* The exact dataset splits producing these results may differ from the dataset splits of this study. However, the same splitting strategies (including the same portions) were used. Furthermore, although these models were fitted to, and predicted on, each dataset three times, only the mean values are reported. Values are directly extracted from the MoleculeNet paper²⁶.

As can be seen in Tables 2 and 3, the GNNs implemented in MolGraph performed as expected as they showed comparable performance to the models of MoleculeNet (*GC*, *Weave*, *MPNN* and *DTNN*). Furthermore, comparing the GNNs of MolGraph, the attentional and message-passing type models seem, overall, to perform marginally better than the convolutional type models. This suggests that increasing the complexity of the models could improve the performance — though at the cost of significantly increasing the computational cost. Although the models (of MolGraph) were run only once against each dataset (one replica), consequently disregarding the variation in performance over replicate runs, it seems that the relative performance of each model heavily depended on the task it tried to solve (which dataset was used). For instance, the GT (graph transformer) models showed impressive performance on the quantum-chemistry datasets (*qm7*, *qm8* and *qm9*), but less so for the physiology datasets (*mu*, *hi*, *pc* and *ba*). An explanation for this could be that the GT models, which use a relatively complex attention mechanism, work well when the molecular graphs are smaller in size (in the case of the quantum-chemistry datasets).

Table 4. Predictive performance on the three chromatography datasets. Bold vs. italic named models visually separate the models (and results) of this study (MolGraph) and models (and results) of other studies (see footnote of table). “(E)” indicates that edge features were used. MRE stands for mean relative error. Convolutional type models: GCN, RGCN(E), GIN, and GraphSage; attentional type models: GAT, GAT(E), GatedGCN, GatedGCN(E), and GMM; and message-passing type models: MPNN(E).

	chromatography				
	SMRT (MRE)	RPLC (MRE)		HILIC (MRE)	
		test	test	external	test
GCN	0.038	0.09	0.13	0.16	0.35
RGCN(E)	0.037	0.11	0.19	0.18	0.33
GIN	0.037	0.10	0.17	0.17	0.30
GraphSage	0.039	0.10	0.15	0.17	0.32
GAT	0.038	0.09	0.15	0.18	0.28
GAT(E)	0.038	0.11	0.16	0.16	0.29
GatedGCN	0.037	0.10	0.15	0.16	0.31
GatedGCN(E)	0.037	0.10	0.14	0.16	0.32
GMM	0.038	0.09	0.15	0.16	0.28
MPNN(E)	0.036	0.10	0.17	0.17	0.37
<i>DLM</i> [*]	<i>0.068</i>	-	-	-	-
<i>Keras</i> [†]	-	<i>0.13</i>	<i>0.18</i>	<i>0.2</i>	<i>0.46</i>

^{*} Values are directly extracted from Domingo-Almenara et al.²⁷ The exact dataset splits producing these results differ from the dataset splits of this study. In their study, a training and test set were used, with 75% and 25% of the data respectively. In this study, a training, validation and test set were used, with 70%, 5% and 25% of the data respectively.

[†] *Keras* refers to the name of the model of Bonini et al.²⁸; a deep fully-connected neural network, implemented in Keras.

Similar to the observations on MoleculeNet (Table 2 and 3), the performance of the GNNs of MolGraph performed as expected on the chromatographic retention time datasets (Table 4). In contrast to the MoleculeNet models, the two models from literature (namely, for SMRT: *DLM*; and for RPLC and HILIC: *Keras*), were not GNNs, but FFNNs. Notably, the FFNNs were based on molecular descriptors — vectors of precomputed features of molecules. It was of interest to compare these *descriptor-based* models (which are commonly used in molecular ML) with the GNNs. Although a direct comparison cannot be made to the DLM (as the exact splitting of the dataset could not be derived), the results of this study indicate superior performance of the GNNs. However, a study by Jiang et al.¹⁰ showed somewhat different results, where descriptor-based models performed comparable to the GNNs on the MoleculeNet datasets.

Molecular identification

In addition to benchmarking the predictive performance of the GNNs of MolGraph on the MoleculeNet datasets, it was also of interest to verify the capabilities of a graph convolutional network (GCN) to assist in molecular identification. For that purpose, a plant metabolite database (PLaSMA, <http://plasma.riken.jp/>) consisting of liquid chromatography-tandem mass spectrometry (LC-MS/MS) data was used. In brief, the identity (structure) of an unknown molecule (analyte) in a given sample can be predicted based on LC-MS/MS data; where the MS/MS data is used to predict

the structure of the analyte (using a software such as MSFinder^{30,31}), and the LC retention times (RTs) are used as an additional confirmation of the proposed structure. Thus, the GCN was trained to correlate the structure of known molecules in the PLaSMA dataset to their associated RTs, and subsequently used to obtain more confidence about proposed structures of analytes. Similar to the benchmarking, the PLaSMA dataset was divided into training, validation and test sets; in which the training set was used to train the model; the validation set was used to supervise the training and to determine thresholds for a *RT filter*; and the test set was used to evaluate how well the GCN model could filter out structures (candidates) suggested by the MSFinder software.

Figure 3 aims to visualize the process of eliminating candidates proposed by MSFinder. The upper plots of Figure 3 illustrate how the validation set was used to define the RT filter (two thresholds, or bounds) that would decide whether a candidate would be discarded (or not) as a possible identity of the analyte. Specifically, if the distance between the predicted RT of the candidate and the RT of the analyte was within the bounds, it was kept, otherwise, discarded. The bounds were defined by the mean and standard deviation of the errors, specifically, $\mu \pm 2.58\sigma$ (-1.313 and 1.337). The bottom subplot of Figure 3 illustrates to what extent the GCN could filter out candidates with the RT filter. As can be seen, a significant portion (about 40%) of the candidates were filtered out (although in specific cases, none, or very few, got filtered out). In one case, a false negative occurred — i.e., the candidate matching the identity of the analyte was discarded. Overall, the results show evidence that the utilization of the GCN for RT predictions may facilitate the process of identifying analytes.

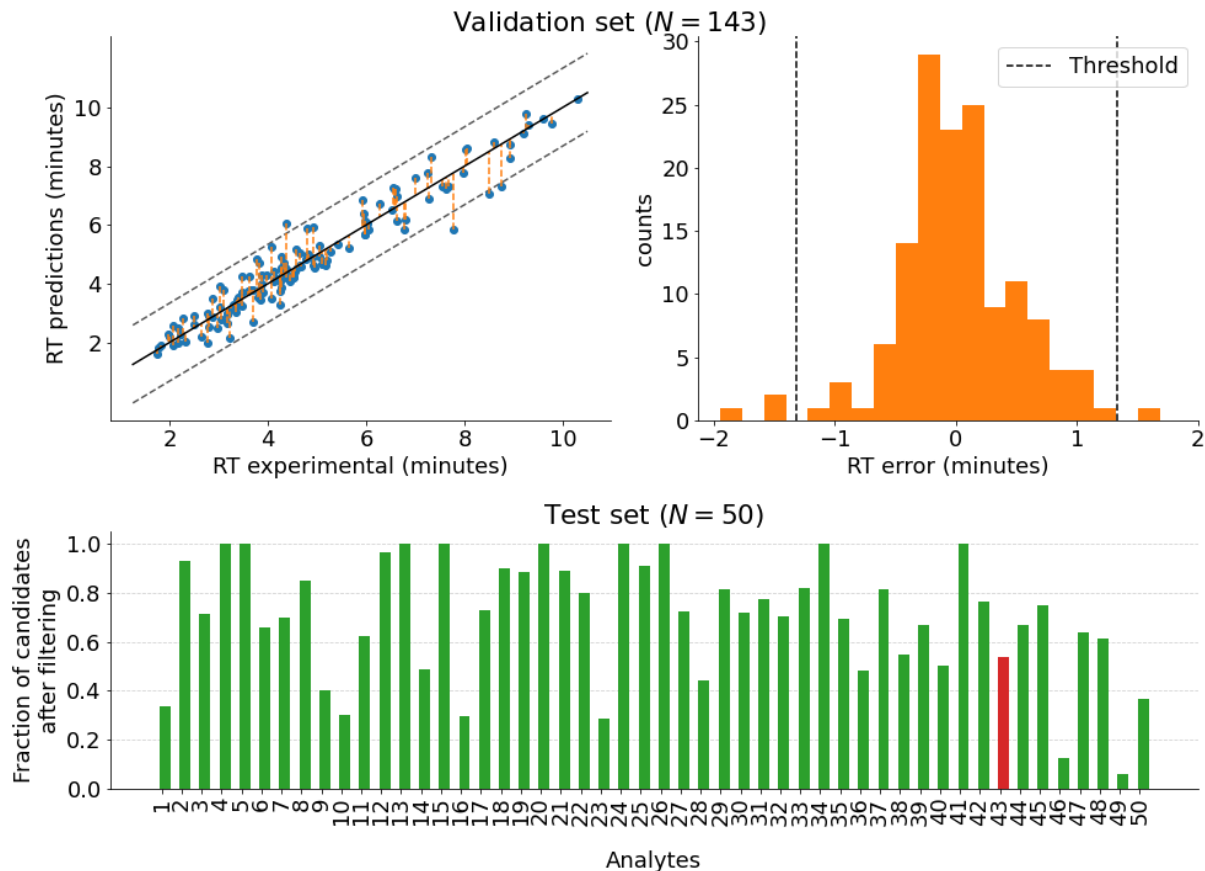


Figure 3. Retention time (RT) filter. Thresholds (-1.313 and 1.337) were computed from the validation set and used to filter out candidates suggested by MSFinder. The red bar indicates a false negative.

To inspect the filtering procedure in more detail, the MSFinder candidate scores as well as predicted candidate RTs (of the GCN), corresponding to analyte 10 (of Figure 3) are shown in Table 5. The candidates highlighted in gray illustrate the candidates that were filtered out by the RT filter; the candidate in bold is the most likely identity based on the MSFinder score and RT filter. In this specific case, the predicted RT proved to be important for correctly identifying the analyte. Comparing MSFinder's three highest scoring candidates and fourth highest scoring candidate (which ended up being the most likely candidate after applying the RT filter), it can be observed that the three highest scoring candidates are significantly more polar — hence low RTs in an RPLC setting. As the analyte had a significantly higher RT (because it was significantly less polar), the RT filter sufficed to discard them. Although this is just a single example, it aims to illustrate how combining information of predicted structures based on MS/MS data and predicted RTs can increase the chances of correctly identifying the analyte.

Table 5. Inspection of analyte 10. In gray: candidates filtered out because of great difference between predicted RTs of candidates vs. the analyte (target) RT. In bold: the most likely identity of the analyte, based on both the MSFinder score and the difference between predicted RT and analyte RT.

Target Identity:	CS(=O)CCCCCCCCN=C=S		
Target RT:	5.41		
Candidates	Score (MSFinder)	Predicted candidate RT	difference
NC(CCOC(=O)CCC(=O)O)C(=O)O	7.32	1.39	4.02
CC(=O)NC1C(=O)OC(CO)C(O)C1O	7.12	1.71	3.70
CC(O)C(=O)NC(CCC(=O)O)C(=O)O	7.06	2.03	3.38
CS(=O)CCCCCCCCN=C=S	7.06	6.07	-0.66
CC(OC(=O)CCC(N)C(=O)O)C(=O)O	6.87	1.63	3.78
Cc1ccc(C=NNc2cn[nH]c(=O)n2)o1	6.73	2.60	2.81
Cc1nonc1NC(=O)Nc1cccn1	5.95	1.94	3.47
CSC=CC(=O)NC=Cc1cccc1	5.78	4.63	0.78
CSC=CNC(=O)C=Cc1cccc1	5.72	4.95	0.46
CCOC(=O)NP(=O)(N1CC1)N1C1	5.34	2.12	3.29

Gradient activation maps

One of the potential strengths of the GNN models is their ability to compute saliency and/or gradient activation maps to better interpret e.g., retention data; i.e., to better understand what substructures contribute to the (retention time) prediction. Figure 4 visualizes four different molecules from the RPLC and HILIC datasets, with gradient activation maps superimposed on 2D structures of these molecules. More contour lines and greener color indicate more importance; i.e., structures that are more important for retention time prediction, relative to substructures with fewer (or no) contour lines. Interestingly, though expectedly, non-polar substructures are clearly most important in the RPLC setting, while polar substructures are clearly most important in the HILIC setting. These results are expected as the non-polar stationary phase of RPLC is expected to interact with the non-polar substructures of the molecules (causing a difference in retention); and similarly,

the polar stationary phase of HILIC is expected to interact with the polar substructures of the molecules. These observations agree with the observations of Kensert et al.⁹, where saliency maps were used (instead of gradient activation maps). However, the advantage of using gradient activation maps over saliency maps, is that the former makes use of the initial node (atom) features as well as the outputted node features of all GNN layers — consequently generating more robust maps.

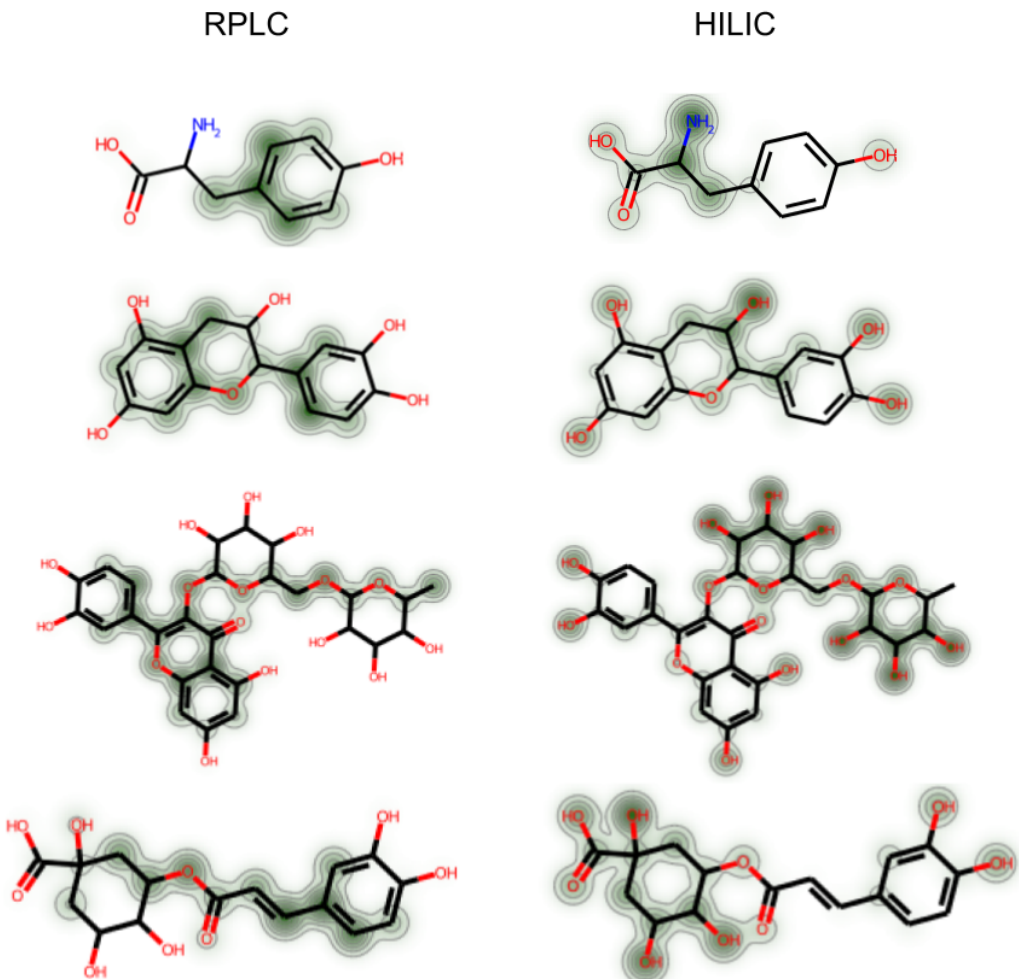


Figure 4. Comparison of gradient activation maps between the RPLC dataset and the HILIC dataset. Gradient activation maps (in green) indicate what substructures were important for the RT prediction.

Conclusions

One of the main motivations behind MolGraph was to develop a GNN package highly compatible with TF and Keras. Consequently, MolGraph's GNNs can be built and utilized with ease — using the TF dataset API for efficient data pipelines, and the Keras sequential (or functional) API for concise implementation of models. MolGraph has an intended limited scope, which on the one hand accommodated an improved chemistry module, but on the other hand limited the capabilities of MolGraph. In prospect, it would be interesting to implement modules for more advanced GNN models, including generative and self-supervised models^{32,33}; and furthermore, to focus on larger graphs, such as proteins and oligonucleotides, which are of great interest in pharmaceutical science^{34,35}.

Acknowledgement

Alexander Kensert is funded by a joint-initiative of the Research Foundation Flanders (FWO) and the Walloon Fund for Scientific Research (FNRS) (EOS – research project “Chimic” (EOS ID: 30897864)).

Conflict of interests

The authors declare that there is no conflict of interest.

References

- (1) Cui, Q.; Lu, S.; Ni, B.; Zeng, X.; Tan, Y.; Chen, Y. D.; Zhao, H. Improved Prediction of Aqueous Solubility of Novel Compounds by Going Deeper With Deep Learning. *Front. Oncol.* **2020**, *10*.
- (2) Wang, Y.-B.; You, Z.-H.; Yang, S.; Yi, H.-C.; Chen, Z.-H.; Zheng, K. A Deep Learning-Based Method for Drug-Target Interaction Prediction Based on Long Short-Term Memory Neural Network. *BMC Med. Inform. Decis. Mak.* **2020**, *20* (2), 49.
- (3) Yuan, Y.; Zheng, F.; Zhan, C.-G. Improved Prediction of Blood–Brain Barrier Permeability Through Machine Learning with Combined Use of Molecular Property-Based Descriptors and Fingerprints. *AAPS J.* **2018**, *20* (3), 54.
- (4) Mauri, A.; Consonni, V.; Todeschini, R. Molecular Descriptors. In *Handbook of Computational Chemistry*; Leszczynski, J., Kaczmarek-Kedziera, A., Puzyn, T., G. Papadopoulos, M., Reis, H., K. Shukla, M., Eds.; Springer International Publishing: Cham, 2017; pp 2065–2093.
- (5) Rogers, D.; Hahn, M. Extended-Connectivity Fingerprints. *J. Chem. Inf. Model.* **2010**, *50* (5), 742–754.
- (6) Kearnes, S.; McCloskey, K.; Berndl, M.; Pande, V.; Riley, P. Molecular Graph Convolutions: Moving beyond Fingerprints. *J. Comput. Aided Mol. Des.* **2016**, *30* (8), 595–608.
- (7) Duvenaud, D.; Maclaurin, D.; Aguilera-Iparraguirre, J.; Gómez-Bombarelli, R.; Hirzel, T.; Aspuru-Guzik, A.; Adams, R. P. Convolutional Networks on Graphs for Learning Molecular Fingerprints. In *Proceedings of the 28th International Conference on Neural Information Processing Systems - Volume 2*; NIPS’15; MIT Press: Cambridge, MA, USA, 2015; pp 2224–2232.
- (8) Gilmer, J.; Schoenholz, S. S.; Riley, P. F.; Vinyals, O.; Dahl, G. E. Neural Message Passing for Quantum Chemistry. In *International Conference on Machine Learning*; PMLR, 2017; pp 1263–1272.
- (9) Kensert, A.; Bouwmeester, R.; Efthymiadis, K.; Van Broeck, P.; Desmet, G.; Cabooter, D. Graph Convolutional Networks for Improved Prediction and Interpretability of Chromatographic Retention Data. *Anal. Chem.* **2021**, *93* (47), 15633–15641.
- (10) Jiang, D.; Wu, Z.; Hsieh, C.-Y.; Chen, G.; Liao, B.; Wang, Z.; Shen, C.; Cao, D.; Wu, J.; Hou, T. Could Graph Neural Networks Learn Better Molecular Representation for Drug Discovery? A Comparison Study of Descriptor-Based and Graph-Based Models. *J. Cheminformatics* **2021**, *13* (1), 12.
- (11) Pope, P. E.; Kolouri, S.; Rostami, M.; Martin, C. E.; Hoffmann, H. Explainability Methods for Graph Convolutional Neural Networks. In *2019 IEEE/CVF Conference on Computer Vision and Pattern Recognition (CVPR)*; 2019; pp 10764–10773.
- (12) Abadi, M.; Agarwal, A.; Barham, P.; Brevdo, E.; Chen, Z.; Citro, C.; Corrado, G. s; Davis, A.; Dean, J.; Devin, M.; Ghemawat, S.; Goodfellow, I.; Harp, A.; Irving, G.; Isard, M.; Jia, Y.; Kaiser, L.; Kudlur, M.; Levenberg, J.; Zheng, X. *TensorFlow : Large-Scale Machine Learning on Heterogeneous Distributed Systems*; 2015.

(13) Chollet, F. Keras, 2015.

(14) Paszke, A.; Gross, S.; Massa, F.; Lerer, A.; Bradbury, J.; Chanan, G.; Killeen, T.; Lin, Z.; Gimelshein, N.; Antiga, L.; Desmaison, A.; Köpf, A.; Yang, E.; DeVito, Z.; Raison, M.; Tejani, A.; Chilamkurthy, S.; Steiner, B.; Fang, L.; Bai, J.; Chintala, S. PyTorch: An Imperative Style, High-Performance Deep Learning Library. *arXiv*.1912.01703.

(15) Grattarola, D.; Alippi, C. Graph Neural Networks in TensorFlow and Keras with Spektral. *arXiv*.2006.12138.

(16) Wang, M.; Zheng, D.; Ye, Z.; Gan, Q.; Li, M.; Song, X.; Zhou, J.; Ma, C.; Yu, L.; Gai, Y.; Xiao, T.; He, T.; Karypis, G.; Li, J.; Zhang, Z. Deep Graph Library: A Graph-Centric, Highly-Performant Package for Graph Neural Networks. *arXiv*.1909.01315.

(17) Ramsundar, B.; Eastman, P.; Walters, P.; Pande, V.; Leswing, K.; Wu, Z. *Deep Learning for the Life Sciences*; O'Reilly Media, 2019.

(18) Fey, M.; Lenssen, J. E. Fast Graph Representation Learning with PyTorch Geometric. *arXiv*.1903.02428.

(19) Battaglia, P. W.; Hamrick, J. B.; Bapst, V.; Sanchez-Gonzalez, A.; Zambaldi, V.; Malinowski, M.; Tacchetti, A.; Raposo, D.; Santoro, A.; Faulkner, R.; Gulcehre, C.; Song, F.; Ballard, A.; Gilmer, J.; Dahl, G.; Vaswani, A.; Allen, K.; Nash, C.; Langston, V.; Dyer, C.; Heess, N.; Wierstra, D.; Kohli, P.; Botvinick, M.; Vinyals, O.; Li, Y.; Pascanu, R. Relational Inductive Biases, Deep Learning, and Graph Networks. *arXiv*.1806.01261.

(20) Schütt, K. T.; Arbabzadah, F.; Chmiela, S.; Müller, K. R.; Tkatchenko, A. Quantum-Chemical Insights from Deep Tensor Neural Networks. *Nat. Commun.* **2017**, *8* (1), 13890.

(21) Kipf, T.; Welling, M. Semi-Supervised Classification with Graph Convolutional Networks. *arXiv*:1609.02907

(22) Dwivedi, V. P.; Joshi, C. K.; Luu, A. T.; Laurent, T.; Bengio, Y.; Bresson, X. Benchmarking Graph Neural Networks. *arXiv*.2003.00982.

(23) Xu, K.; Hu, W.; Leskovec, J.; Jegelka, S. How Powerful Are Graph Neural Networks? *arXiv*.1810.00826.

(24) Veličković, P.; Cucurull, G.; Casanova, A.; Romero, A.; Liò, P.; Bengio, Y. Graph Attention Networks. *arXiv*.1710.10903.

(25) Monti, F.; Boscaini, D.; Masci, J.; Rodolà, E.; Svoboda, J.; Bronstein, M. M. Geometric Deep Learning on Graphs and Manifolds Using Mixture Model CNNs. *arXiv*.1611.08402.

(26) Wu, Z.; Ramsundar, B.; Feinberg, E. N.; Gomes, J.; Geniesse, C.; Pappu, A. S.; Leswing, K.; Pande, V. MoleculeNet: A Benchmark for Molecular Machine Learning. *Chem. Sci.* **2017**, *9* (2), 513–530.

(27) Domingo-Almenara, X.; Guijas, C.; Billings, E.; Montenegro-Burke, J. R.; Uritboonthai, W.; Aisporna, A. E.; Chen, E.; Benton, H. P.; Siuzdak, G. The METLIN Small Molecule Dataset for Machine Learning-Based Retention Time Prediction. *Nat. Commun.* **2019**, *10* (1), 5811.

(28) Bonini, P.; Kind, T.; Tsugawa, H.; Barupal, D. K.; Fiehn, O. Retip: Retention Time Prediction for Compound Annotation in Untargeted Metabolomics. *Anal. Chem.* **2020**, *92* (11), 7515–7522.

(29) Kingma, D. P.; Ba, J. Adam: A Method for Stochastic Optimization. *arXiv*:1412.6980.

(30) Tsugawa, H.; Kind, T.; Nakabayashi, R.; Yukihira, D.; Tanaka, W.; Cajka, T.; Saito, K.; Fiehn, O.; Arita, M. Hydrogen Rearrangement Rules: Computational MS/MS Fragmentation and Structure Elucidation Using MS-FINDER Software. *Anal. Chem.* **2016**, *88* (16), 7946–7958.

(31) Lai, Z.; Tsugawa, H.; Wohlgemuth, G.; Mehta, S.; Mueller, M.; Zheng, Y.; Ogiwara, A.; Meissen, J.; Showalter, M.; Takeuchi, K.; Kind, T.; Beal, P.; Arita, M.; Fiehn, O. Identifying Metabolites by Integrating Metabolome Databases with Mass Spectrometry Cheminformatics. *Nat. Methods* **2018**, *15* (1), 53–56.

(32) De Cao, N.; Kipf, T. MolGAN: An Implicit Generative Model for Small Molecular Graphs. *arXiv*.1805.11973.

(33) Hu, W.; Liu, B.; Gomes, J.; Zitnik, M.; Liang, P.; Pande, V.; Leskovec, J. Strategies for Pre-Training Graph Neural Networks. *arXiv*.1905.12265.

- (34) Kesik-Brodacka, M. Progress in Biopharmaceutical Development. *Biotechnol. Appl. Biochem.* **2018**, *65* (3), 306–322.
- (35) Roberts, T. C.; Langer, R.; Wood, M. J. A. Advances in Oligonucleotide Drug Delivery. *Nat. Rev. Drug Discov.* **2020**, *19* (10), 673–694.